Journal of Zhejiang University-SCIENCE C (Computers & Electronics)
ISSN 1869-1951 (Print); ISSN 1869-196X (Online)
www.zju.edu.cn/jzus; www.springerlink.com
E-mail: jzus@zju.edu.cn

Analysis of vibration reduction level in an 8/6 switched reluctance machine by active vibration cancellation

Xu LIU[1,2], Zai-ping PAN[†‡1], Z. Q. ZHU[1,2]

([1]*School of Electrical Engineering, Zhejiang University, Hangzhou 310027, China*)

([2]*Department of Electronic and Electrical Engineering, University of Sheffield, Sheffield S1 3JD, UK*)

[†]E-mail: panzaiping@zju.edu.cn

Received Nov. 13, 2009; Revision accepted Mar. 5, 2010; Crosschecked Sept. 3, 2010

Abstract: This paper proposes an analytical model for predicting the maximum vibration reduction level in a four-phase 8/6 switched reluctance machine (SRM) by employing active vibration cancellation (AVC), one of the most effective and convenient methods for reducing the vibration and acoustic noise produced by SRMs. Based on the proposed method, the factors that influence the vibration reduction level are analyzed in detail. The relationships between vibration and noise reduction levels at resonance frequency and rotor speed are presented. Moreover, it is shown that a large damping factor will lead to smaller vibration reduction level with AVC while, in contrast, a large resonance frequency will increase the vibration reduction level. Both finite element analyses and experiments were carried out on a prototype 8/6 SRM to validate the proposed method.

Key words: Active vibration cancellation, Analytical model, Switched reluctance machine, Vibration
doi:10.1631/jzus.C0910697 **Document code:** A **CLC number:** TM301.4

1 Introduction

Switched reluctance machines (SRMs) have been used in some industry applications, including starter-generators for aircraft, electric vehicles, and underground mining conveyors. In some applications noise and vibration are not critical and the robustness, reliability, and lower cost that SRMs can provide are more important considerations. Moreover, as there is no magnet or winding in the rotor, SRMs are very suitable for harsh environments or high speed applications. Nevertheless, the large vibration level and high noise emission are the main drawbacks that limit the wide application of SRMs.

To reduce the vibration in SRMs, some valuable suggestions have been proposed from the perspective of machine design, such as increasing the back iron (Colby *et al.*, 1996; Long *et al.*, 2001), applying an auxiliary winding to suppress the radial force by injecting harmonic currents (Lecointe *et al.*, 2004), or designing with an optimal rib structure (Sun *et al.*, 2007). However, owing to the variable speed application of SRMs it is impossible to avoid resonance during its operation. Therefore, attempts have been made to improve the control strategy with hybrid excitation (Ahn *et al.*, 2004), using random frequency pulse width modulation (PWM), turn-on and turn-off angles, current-tail profile shaping (Gabsi *et al.*, 1999; Chai *et al.*, 2006), or by optimizing the turn-on and turn-off angles through experiment transfer functions and response surface methodology (Ha *et al.*, 2004). However, these methods require additional experiments (Cai *et al.*, 2002) or finite element analysis (FEA) calculations (Tang, 1997; Srinivas and Arumugam, 2004), which are time consuming and add more cost.

One effective way of reducing the vibration and noise emission of SRMs is to employ active vibration cancellation (AVC) by simply introducing a two-step voltage control with a constant period of zero voltage excitation (a half cycle of dominant natural frequency) (Pollock and Wu, 1997; Long *et al.*, 2005). However,

‡ Corresponding author

these studies were focused in the time domain and were illustrated by experiments (Wu and Pollock, 1995). Furthermore, there is no method for quantifying the maximum level of noise and vibration reduction which an AVC can achieve, and existing methods cannot determine which factors will influence the vibration reduction level. Therefore, in this paper an analytical method is proposed for calculating the maximum reduction level in a prototype 8/6 SRM and is validated by both finite element analyses and experiments. Further, from the developed analytical method, the factors that may influence the vibration reduction level are analyzed in detail.

2 Principle of active vibration cancellation

The widely used inverter for driving SRMs is the asymmetric bridge (of which only one phase leg is shown in Fig. 1 as other phases have the same configuration). The stator deformation at turn-off is dominant to that at turn-on (Cameron *et al*., 1992; Colby *et al.*, 1996). However, in the conventional excitation scheme, both switches S_1 and S_2 are turned off simultaneously, and then the phase current passes through two diodes, as illustrated by the path ②, which makes the phase voltage change from U_0 to $-U_0$ (Miller, 1993). During this period a decayed free oscillating vibration is provoked in the corresponding phase.

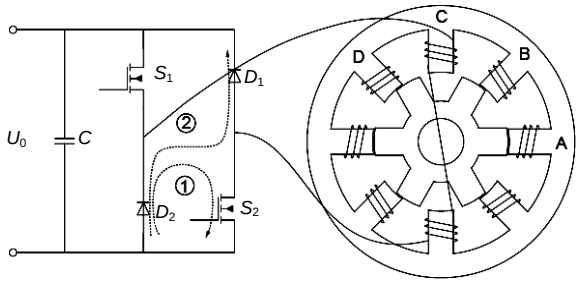

Fig. 1 A four-phase 8/6 switched reluctance machine and one phase leg of an asymmetric bridge inverter

However, by applying AVC the turn-off procedure is divided into two steps: firstly, only the upper leg switch is turned off, which will make the phase voltage change from only U_0 to zero (Fig. 1①). Consequently, the amplitude of induced vibration will be only half of that in the conventional switching method. Further, after about half of a resonant cycle the lower leg switch S_2 is turned off, which provokes another vibration which is out of phase with the previous one. As a result, the vibration after half of a resonant cycle will be greatly suppressed (Fig. 2).

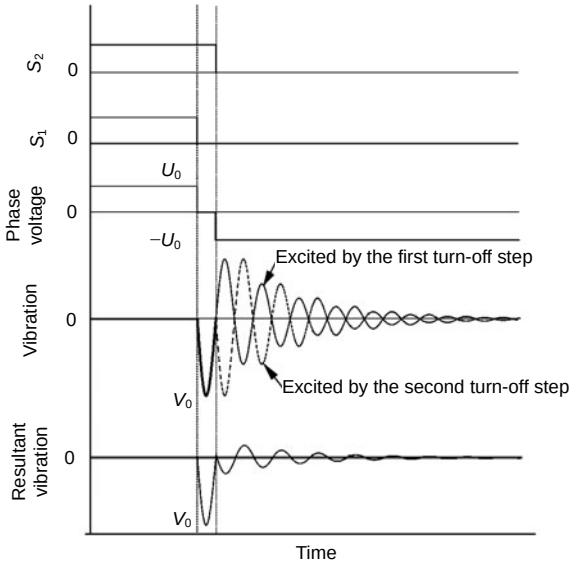

Fig. 2 The principle of active vibration cancellation

3 Analytical model for predicting vibration reduction in an 8/6 SRM

3.1 Conventional excitation

In conventional excitation, the phase windings are excited one by one. Therefore, the vibration outside the magnetic pole will not only be provoked by the current through each winding itself, but also be generated by the current of other phases. Fig. 3 illustrates the elliptic deformation in an 8/6 SRM when the phase C is excited.

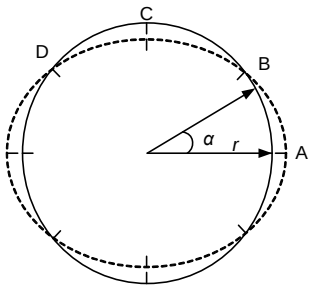

Fig. 3 Elliptic deformation in an 8/6 switched reluctance machine

Therefore, the vibrations in phases A, B, C, D (V_a, V_b, V_c, V_d) are the sum of the individual vibrations generated by each phase separately (V_{aa}, V_{bb}, V_{cc}, V_{dd}), that is,

$$\begin{bmatrix} V_{\mathrm{a}} \\ V_{\mathrm{b}} \\ V_{\mathrm{c}} \\ V_{\mathrm{d}} \end{bmatrix} = \begin{bmatrix} 1 & 0 & -1 & 0 \\ 0 & 1 & 0 & -1 \\ -1 & 0 & 1 & 0 \\ 0 & -1 & 0 & 1 \end{bmatrix} \begin{bmatrix} V_{\mathrm{aa}} \\ V_{\mathrm{bb}} \\ V_{\mathrm{cc}} \\ V_{\mathrm{dd}} \end{bmatrix}, \tag{1}$$

in which

$$\begin{bmatrix} V_{\mathrm{aa}} \\ V_{\mathrm{bb}} \\ V_{\mathrm{cc}} \\ V_{\mathrm{dd}} \end{bmatrix} = \begin{bmatrix} V(t,\alpha=0) \\ V(t,\alpha=\pi/4) \\ V(t,\alpha=\pi/2) \\ V(t,\alpha=3\pi/4) \end{bmatrix}. \tag{2}$$

Therefore, the vibration outside each magnetic pole in an 8/6 SRM is as shown in Fig. 4. In one commutation cycle, the vibration outside each magnetic pole has two oscillations, one provoked by itself, and another generated by the phase which is positioned at 90° to it. Each one can be written as

$$V_{\mathrm{aa}} = V(t,\alpha=0) = -2V_0 \mathrm{e}^{-ct} \sin(2\pi t / T_0), \tag{3}$$

where c stands for the damping factor, T_0 is the dominant mechanical resonant cycle, and V_0 is half of the amplitude of vibration. However, the two oscillations are out of phase, and the cycle T is determined by the rotor speed. Owing to the periodicity of the vibration, the vibration outside the magnetic pole resulting from its own excitation can be written as

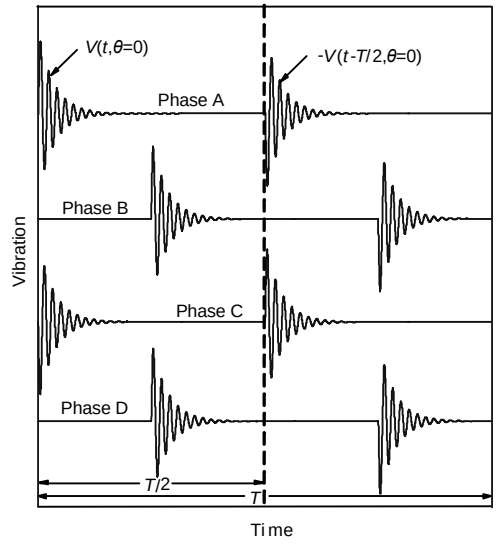

Fig. 4 Schematic diagram of stator vibration under conventional excitation

$$V_{\mathrm{aa}}(t,\alpha=0) = \frac{a_n}{2} + \sum_{n=1}^{\infty}\left(a_n \cos\left(\frac{2n\pi}{T}t\right) + b_n \sin\left(\frac{2n\pi}{T}t\right)\right), \tag{4}$$

where the coefficients a_n and b_n are given by

$$\begin{aligned} a_n &= \frac{2}{T}\int_0^T -2V_0 \mathrm{e}^{-ct} \sin\left(\frac{2\pi}{T_0}t\right)\cos\left(\frac{2n\pi}{T}t\right)\mathrm{d}t \\ &= -2T_0V_0\left\{\frac{1}{(cTT_0)^2+(2\pi(T-nT_0))^2}\left[2\pi(T-nT_0)\right.\right. \\ &\quad -\mathrm{e}^{-cT}\left(2\pi(T-nT_0)\cos\left(\frac{2\pi(T-nT_0)}{T_0}\right)\right. \\ &\quad \left.\left.+cTT_0\sin\left(\frac{2\pi(T-nT_0)}{T_0}\right)\right)\right] \\ &\quad +\frac{1}{(cTT_0)^2+(2\pi(T+nT_0))^2}\left[2\pi(T+nT_0)\right. \\ &\quad -\mathrm{e}^{-cT}\left(2\pi(T+nT_0)\cos\left(\frac{2\pi(T+nT_0)}{T_0}\right)\right. \\ &\quad \left.\left.\left.+cTT_0\sin\left(\frac{2\pi(T+nT_0)}{T_0}\right)\right)\right]\right\}, \end{aligned} \tag{5}$$

$$\begin{aligned} b_n &= \frac{2}{T}\int_0^T -2V_0 \mathrm{e}^{-ct} \sin\left(\frac{2\pi}{T_0}t\right)\sin\left(\frac{2n\pi}{T}t\right)\mathrm{d}t \\ &= -2T_0V_0\left\{\frac{1}{(cTT_0)^2+(2\pi(T-nT_0))^2}\right. \\ &\quad \cdot\left[cTT_0+\mathrm{e}^{-cT}\left(-cTT_0\cos\left(\frac{2\pi(T-nT_0)}{T_0}\right)\right.\right. \\ &\quad \left.\left.+2\pi(T-nT_0)\sin\left(\frac{2\pi(T-nT_0)}{T_0}\right)\right)\right] \\ &\quad +\frac{1}{(cTT_0)^2+(2\pi(T+nT_0))^2} \\ &\quad \cdot\left[-cTT_0+\mathrm{e}^{-cT}\left(cTT_0\cos\left(\frac{2\pi(T+nT_0)}{T_0}\right)\right.\right. \\ &\quad \left.\left.\left.-2\pi(T+nT_0)\sin\left(\frac{2\pi(T+nT_0)}{T_0}\right)\right)\right]\right\}. \end{aligned} \tag{6}$$

Therefore, the resultant vibration provoked by the excitation of its own phase and the other phase (Fig. 4) is

$$V(t)=V_1(t)-V_1\left(t-\frac{T}{2}\right)$$
$$=\frac{a_0}{2}+\sum_{n=1}^{\infty}\left(a_n\cos\left(\frac{2n\pi}{T}t\right)+b_n\sin\left(\frac{2n\pi}{T}t\right)\right)$$
$$-\left(\frac{a_0}{2}+\sum_{n=1}^{\infty}\left(a_n\cos\left(\frac{2n\pi}{T}\left(t-\frac{T}{2}\right)\right)+b_n\sin\left(\frac{2n\pi}{T}\left(t-\frac{T}{2}\right)\right)\right)\right)$$
$$=\sum_{n=1}^{\infty}\left(a'_n\cos\left(\frac{2n\pi}{T}t\right)+b'_n\sin\left(\frac{2n\pi}{T}t\right)\right), \quad (7)$$

where

$$a'_n=\begin{cases}2a_n, & n=2k-1\ (k=1,2,\cdots),\\ 0, & n=2k\ (k=1,2,\cdots),\end{cases} \quad (8)$$

$$b'_n=\begin{cases}2b_n, & n=2k-1\ (k=1,2,\cdots),\\ 0, & n=2k\ (k=1,2,\cdots).\end{cases} \quad (9)$$

Therefore, the amplitude of each frequency component is

$$A_n=\begin{cases}2\sqrt{a_n^{\,2}+b_n^{\,2}}, & n=2k-1\ (k=1,2,\cdots),\\ 0, & n=2k\ (k=1,2,\cdots).\end{cases} \quad (10)$$

3.2 Active vibration cancellation

Based on the model described in Section 2, the vibration after half a resonant cycle is very small and can be neglected. Therefore, the vibration after applying AVC can be considered as only the first half cycle of the vibration remaining (Fig. 5). Hence, the overall vibration outside the magnetic pole of phase C can be expressed as

$$V(t+T_0/2)=\begin{cases}-V_0\cos\left(\frac{2\pi}{T_0}t\right), & 0\le t\le\frac{T_0}{4},\\ V_0\cos\left(\frac{2\pi}{T_0}\left(t-\frac{T}{2}\right)\right), & \frac{T}{2}-\frac{T_0}{4}\le t\le\frac{T}{2}+\frac{T_0}{4},\\ -V_0\cos\left(\frac{2\pi}{T_0}(t-T)\right), & T-\frac{T_0}{4}\le t\le T,\\ 0, & \text{otherwise},\end{cases} \quad (11)$$

which can also be expressed as Fourier series:

$$V(t+T_0/2)=\sum_{n=1}^{\infty}a_n\cos\left(\frac{2n\pi}{T}t\right), \quad (12)$$

where the coefficient a_n is

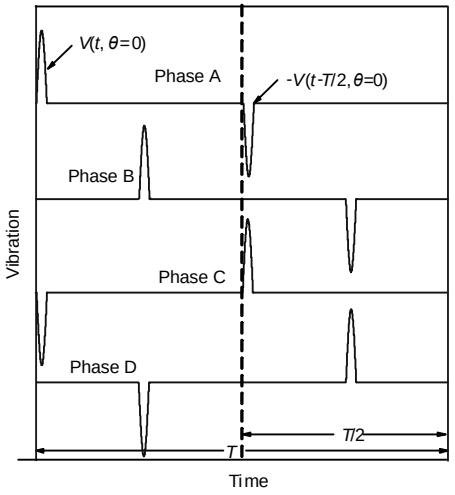

Fig. 5 Schematic diagram of stator vibration by applying active vibration cancellation (AVC)

$$a_n=\frac{2}{T}\int_0^T v(t)\cos\left(\frac{2n\pi}{T}t\right)\mathrm{d}t$$
$$=\frac{\frac{T_0}{T}V_0\cos\left(\frac{n\pi T_0}{2T}\right)\cdot\left(-2+2\cos(n\pi)\right)}{\pi\left(1-\left(nT_0/T\right)^2\right)}. \quad (13)$$

The amplitude of each frequency component, A_n, is equal to the coefficient a_n. Comparing the vibration with and without AVC, it can be seen that the amplitude will be zero when n is an even number, and that the damping factor has little influence on the vibration with AVC while it affects the amplitude of each frequency component in conventional excitation. Another difference between the two excitations is the vibration amplitude. By applying AVC the voltage change and the vibration amplitude are halved.

However, it is more important to consider the amplitude at resonant frequency than the amplitude at other frequencies. Hence, it is important to analyze the vibration reduction at this frequency.

4 Maximum reduction level of vibration around resonance frequency in an 8/6 SRM

In conventional excitation, the vibration around the resonance frequency is significant, no matter which control method is applied. Although the amplitude of vibration V_0 is determined by the phase current, it will be cancelled out in calculating the

vibration reduction level. In general, the phase current is related to the load. At heavy load the phase current and the consequent vibration will also be larger.

Moreover, since the two-step turn-off procedure in AVC has little influence on the phase current profile (Pollock and Wu, 1997; Long *et al*., 2005), the comparison with and without AVC can be carried out under similar conditions. To obtain the vibration level at resonance frequency under both excitations, the index n in Eqs. (10) and (13) needs to be determined first, i.e.,

$$n_0 = \left[\frac{T}{T_0}\right] = \left[\frac{60\pi}{p\omega T_0}\right], \tag{14}$$

in which n_0 is equal to the integer nearest to T/T_0, and p and ω stand for pole pairs and angular velocity per minute, respectively. Substituting Eq. (14) into Eqs. (5) and (6), the peak value of vibration at resonant frequency without AVC can be obtained as

$$A_{n0} = \frac{V_0 T_0 p\omega}{15\pi}\sqrt{a_{n0}^2 + b_{n0}^2}, \tag{15}$$

in which a_{n0} and b_{n0} are given by

$$a_{n0} = \frac{2\mathrm{e}^{-cT} - 4\pi}{(cT_0)^2 + (4\pi)^2}, \tag{16}$$

$$b_{n0} = \frac{\mathrm{e}^{-cT} - 1}{cT_0} + \frac{cT_0 - cT_0\mathrm{e}^{-cT}}{(cT_0)^2 + (4\pi)^2}. \tag{17}$$

Similarly, the peak value of vibration at resonant frequency with AVC can be derived as follows:

$$A_{n0} = \lim_{T \to n_0 T_0} a_n = \frac{V_0}{n_0}, \tag{18}$$

i.e.,

$$A_{n0} = \frac{V_0 T_0 p\omega}{60\pi}. \tag{19}$$

Therefore, the vibration reduction level around the resonance frequency can be written as

$$\begin{aligned}\Delta L_V &= 20\lg\left(\frac{V_0 T_0 p\omega}{15\pi}\sqrt{a_{n0}^2 + b_{n0}^2}\right) - 20\lg\left(\frac{V_0 T_0 p\omega}{60\pi}\right)\\ &= 20\lg\left(4\sqrt{a_{n0}^2 + b_{n0}^2}\right).\end{aligned} \tag{20}$$

Eq. (20) shows that the vibration reduction level around the resonance frequency is determined mainly by the coefficients a_{n0} and b_{n0} and is independent of V_0, T_0, and p. But it relates to the rotor speed, the damping factor, and the resonance frequency. The rotor speed will change mainly the cycle period T, while at low speed, because the damping factor c is relatively large, the term e^{-cT} is almost zero, as we will discuss later. The damping factor and resonance frequency are predetermined during the motor design procedure. Therefore, for a predefined motor the coefficients a_{n0} and b_{n0} are mostly influenced by the rotor speed.

5 Simulation and experimental verification

To verify the proposed analytical method for calculating the maximum vibration reduction level, finite element analyses and experiments were carried out on a typical 8/6 SRM with geometric dimensions as listed in Table 1.

From the 2D FEA, the resonance frequency of dominant vibration mode 2 in an 8/6 SRM is 2193.98 Hz. In the finite element calculation, Young's modulus and Poisson's ratio were set to 2×10^{11} Pa and 0.3, respectively. For simplicity, the influences of windings and end-caps were not considered. This will not lead to any problem since the resonant frequency of the SRM was also measured, as will be shown later, and used for subsequent implementation of AVC. To verify the analysis that the vibration outside the stator pole is generated only by the excitation of the corresponding phase and the phase which is at 90° to it, the stator deformation under one phase excitation is illustrated in Fig. 6. Compared with the analytical model in Fig. 3, owing to the thickness of the stator back-iron, the excitation of one phase invokes mainly the deformation outside its pole and the phase pole which is at 90° to it, while the deformation outside other stator poles is negligible. Note that the deformation outside the excitation phase pole is slightly higher than that which is 90° apart. Furthermore, they have opposite deformation directions, since the order of dominant vibration mode is 2. Fig. 6 shows the deformation of a prototype 8/6 SRM with an external force (5000 N/mm^2) exerted on the poles of phase C, which is equivalent to a current density of 1.22 A/mm^2 excited in windings of phase C at the aligned position.

Table 1 Parameters of the prototype 8/6 switched reluctance machine (SRM)

Parameter	Value
Geometric parameters	
Stator outer diameter	93.8
Rotor diameter	46.9
Air gap	0.5
Stack length	46.9
Stator pole arc	21°
Rotor pole arc	23°
Electric parameters	
Number of phases	4
Nominal voltage	24 V
Rated speed	1000 r/min
Rated power	200 W

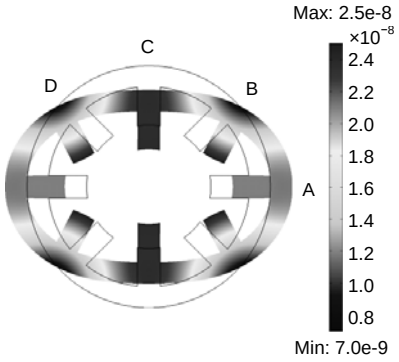

Fig. 6 Deformation with phase C winding excitation (excitation force=5000 N/m^2)

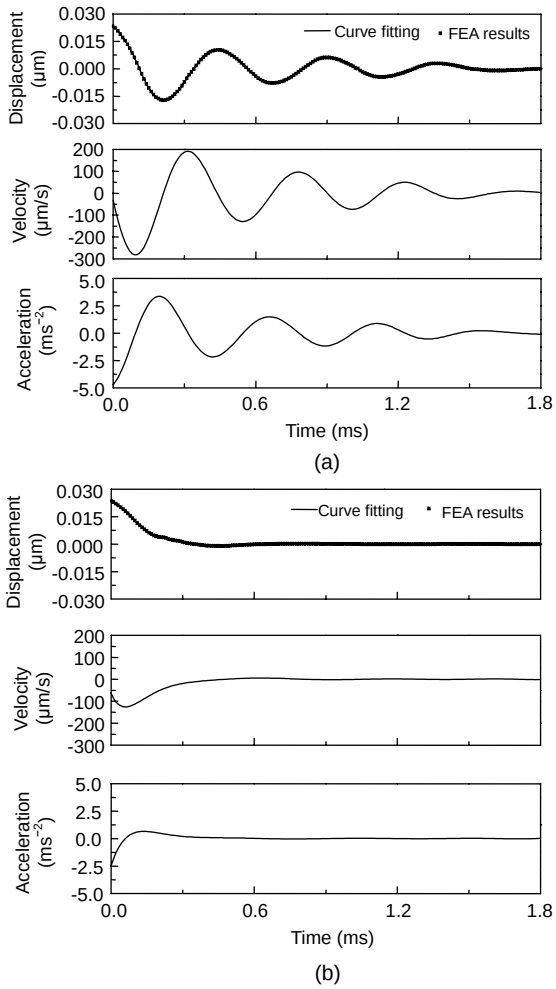

Fig. 7 Transient finite element analysis (FEA) results of a prototype 8/6 switched reluctance machine (SRM) outside the excited stator pole (initial force on the excited pole is 5000 N/m^2)

(a) Displacement, velocity, and acceleration without applying active vibration cancellation (AVC); (b) Displacement, velocity, and acceleration with AVC applied

To illustrate the vibration behavior outside the excited stator pole, take the case of Fig. 6 as the initial condition, and then release the exerted force. The corresponding simulation results are shown in Figs. 7a and 7b without and with AVC respectively, from which it can be seen that after AVC is applied the magnitude of vibration is reduced by half, as expected.

To further verify the analytical model for predicting the vibration reduction level, experiments were carried out on a prototype 8/6 SRM. An accelerometer with an output sensitivity of 1000 mV/g was attached outside the stator pole in the middle of the frame along the axial direction (Fig. 8).

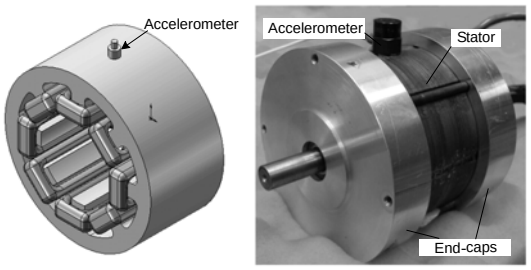

Fig. 8 Location of accelerometer (outside the stator pole of phase C)

To determine the natural frequencies of the SRM, impulse tests were carried out to identify the resonance frequency of dominant vibration mode 2. Fig. 9 shows the impulse force vibration response of the prototype 8/6 SRM, which shows the frequency of vibration mode 2 was about 2148 Hz. Therefore, the zero voltage period between two turn-off instants should be 228.9 μs, which is half of the dominant resonant period, so as to implement the AVC. Fig. 10

shows the system configuration for implementing the AVC, in which the prototype SR motor is operated under single pulse mode. The delay cycle is realized via a timer in the controller. As soon as the commutation begins, the timer is reset to zero and starts to count. As soon as the timer reaches half the dominant resonant period, the lower leg switch is turned off. Fig. 11 compares the vibrations outside the stator pole with and without AVC in the time domain at a speed of 1000 r/min. Each phase is turned on at 0°, which is defined as the unaligned position associated with the phase, and remains on for a duration of 15° (mechanical angle).

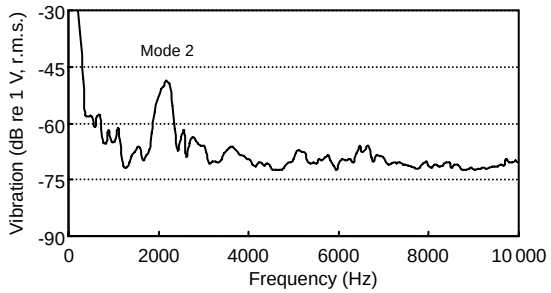

Fig. 9 Impulse force vibration response of a prototype 8/6 switched reluctance machine (SRM)

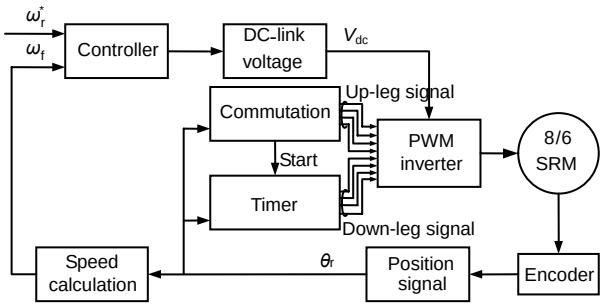

Fig. 10 Configuration of an 8/6 switched reluctance machine (SRM) drive for implementing active vibration cancellation (AVC)

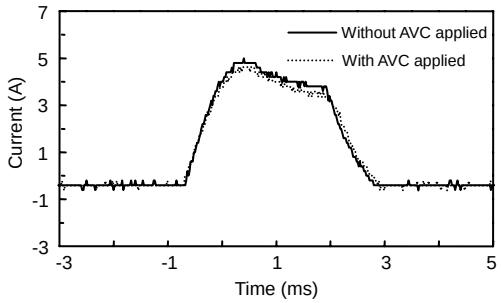

Fig. 11 Measured phase current comparison at speed of 1000 r/min with and without active vibration cancellation (AVC) applied

Fig. 11 shows the phase current waveform with and without AVC, from which it can be seen that with AVC applied, the turn-off period will be slightly longer. However, the influence on the phase current waveform is insignificant since the resonance frequency (mode 2) of the prototype 8/6 SRM was much larger than that of commutation, which leads to a very small zero period between two turn-off procedures. Therefore, the implementation of AVC will have little impact on the torque production. Fig. 12 shows the vibration responses outside the stator pole with and without AVC in the time domain, under 0.4 N·m and single pulse voltage control. The corresponding excitation current waveforms are shown in Fig. 11. The maximum acceleration outside the excited pole without applying AVC was 4.707 ms^{-2}, while that with AVC applied was 2.096 ms^{-2}. By applying AVC the vibration has been successfully suppressed, and the amplitude attributed to the AVC is about half of that under conventional excitation. This also verifies the assumption with AVC in the analytical method for predicting the vibration reduction level.

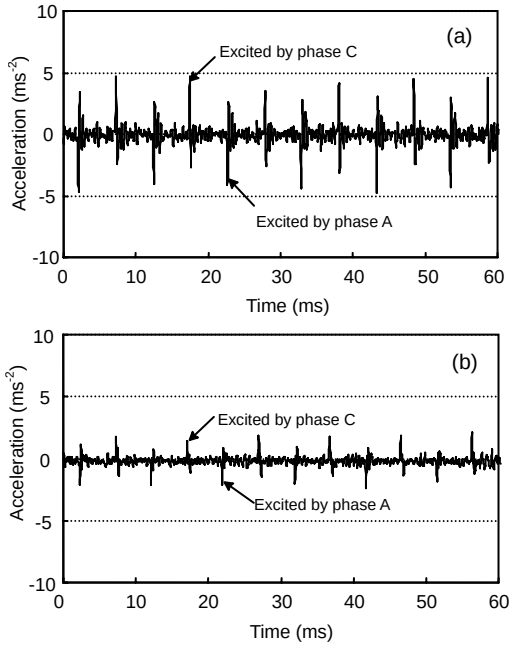

Fig. 12 Measured vibration response in the time domain at a speed of 1000 r/min with (a) and without (b) active vibration cancellation (AVC) applied

Fig. 13 compares the vibration spectra with and without applying AVC at a speed of 1000 r/min. The vibration peak around the resonance frequency of vibration mode 2 has been eliminated with AVC. The

noise was also tested using a microphone at a distance of 40 mm from the surface of the prototype 8/6 SRM. The noise spectra results with and without applying AVC are shown in Fig. 14. To investigate the relationship between the vibration level and the rotor speed with and without AVC applied, the vibration levels at different speeds but at constant load were measured (Fig. 15). The results verify the proposed analytical method in that no matter whether AVC is used the vibration level is proportional to the rotor speed.

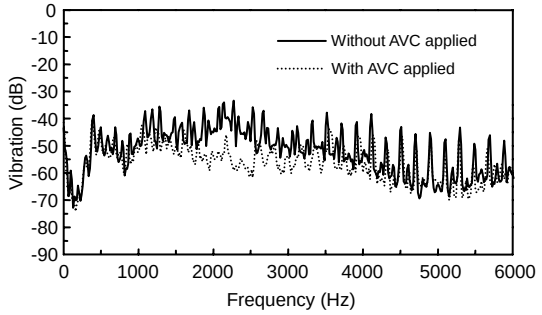

Fig. 13 Measured vibration spectra comparison at a speed of 1000 r/min with and without active vibration cancellation (AVC) applied

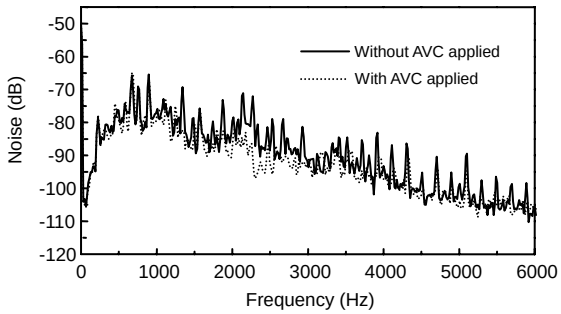

Fig. 14 Measured noise spectra comparison at a speed of 1000 r/min with and without active vibration cancellation (AVC) applied

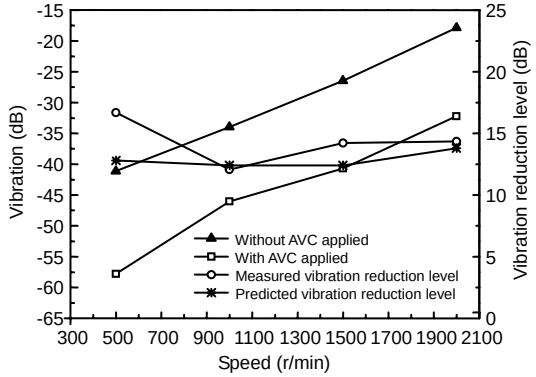

Fig. 15 Vibration level and vibration reduction level at resonance frequency (mode 2) at different speeds

To verify the proposed analytical method for calculating the vibration reduction level, the damping factor (1953.6) was determined by curve fitting with experimental results. The vibration levels at resonance frequency (mode 2) calculated by the proposed analytical method and the measured results show good agreement (Fig. 15). It can also be seen that owing to the large damping factor at relatively low rotor speed, the vibration reduction level at resonant frequency did not change much. As the rotor speed increases, the cycle T will decrease, and thus the vibration reduction level at the resonance frequency will reduce as well. However, in the prototype 8/6 SRM, because of the relatively large damping factor, the term e^{-cT} in Eqs. (16) and (17) is only 4.7e-14 at a speed of 2000 r/min, and will be 0.0022 at speeds up to 10 000 r/min. Therefore, the vibration reduction level at resonance frequency can be considered as constant. Moreover, the noise level at a distance of 40 mm from the motor surface also agrees with the vibration reduction level at resonance frequency (Fig. 16).

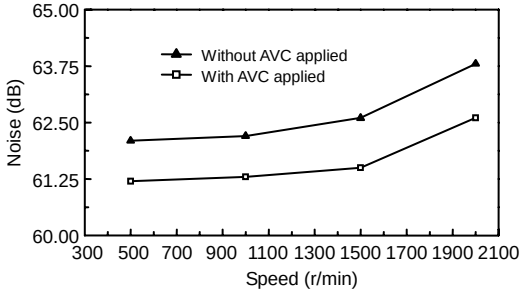

Fig. 16 Measured noise level at a distance of 40 mm away from the surface of the prototype switched reluctance machine (SRM)with and without active vibration cancellation (AVC) applied

Moreover, from Eqs. (16) and (17) it can be seen that the reduction level is also related to the damping factor and the resonance frequency. Therefore, it is also important to investigate the relationship between the vibration reduction level with AVC and these parameters, which can provide a method for low vibration and low noise SRM design incorporating AVC. Fig. 17 shows the vibration reduction level plotted against the damping factor and the resonance frequency. As the scale of the damping factor increases between 1000 and 4000, the vibration reduction level will reduce, and a larger vibration reduction level will be achieved with a higher resonance frequency from 1000 Hz to 5000 Hz.

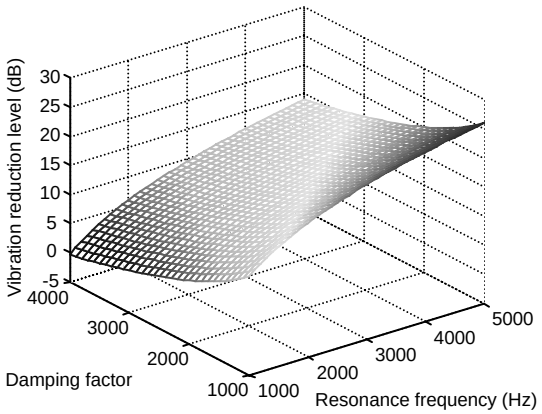

Fig. 17 Vibration reduction level with and without active vibration cancellation (AVC) plotted against resonance frequency and damping factor at 1000 r/min

6 Conclusions

In this paper we have developed an analytical method for predicting the vibration reduction level in four-phase 8/6 SRMs. The analytical expressions for calculating the vibration level with and without AVC applied are derived, and the vibration reduction level around the resonant frequency is also presented. The factors that can influence the vibration reduction level with and without AVC applied are also analyzed. To verify the proposed analytical method, both FEA and experiments were carried out to predict the vibration responses and spectra in a prototype 8/6 SRM with and without AVC applied. Good agreement between predictions and results was achieved.

Acknowledgements

The first author thanks the University of Sheffield, UK, for financial support during a one-year visiting studentship.

References

Ahn, J.W., Park, S.J., Lee, D.H., 2004. Hybrid excitation of SRM for reduction of vibration and acoustic noise. *IEEE Trans. Ind. Electron.*, **51**(2):374-380. [doi:10.1109/TIE.2004.825227]

Cai, W., Pillay, P., Tang, Z., 2002. Impact of stator windings and end-bells on resonant frequencies and mode shapes of switched reluctance motors. *IEEE Trans. Ind. Appl.*, **38**(4):1027-1036. [doi:10.1109/TIA.2002.800594]

Cameron, D.E., Lang, J.J., Umans, S.D., 1992. The origin and reduction of acoustic noise in double salient variable reluctance motor. *IEEE Trans. Ind. Appl.*, **28**(6):1250-1255. [doi:10.1109/28.175275]

Chai, J.Y., Lin, Y.W., Liaw, C.M., 2006. Comparative study of switching control in vibration and acoustic noise reductions for switched reluctance motor. *IEE Proc.-Electr. Power Appl.*, **153**(3):348-360. [doi:10.1049/ip-epa:20050340]

Colby, R.S., Mottier, F.M., Miller, T.J.E., 1996. Vibration modes and acoustic noise in a four-phase switched reluctance motor. *IEEE Trans. Ind. Appl.*, **32**(6):1357-1364. [doi:10.1109/28.556639]

Gabsi, M., Camus, F., Loyau, T., Barbry, J.L., 1999. Noise Reduction of Switched Reluctance Motor. Int. Conf. Electric Machines and Drives, p.263-265. [doi:10.1109/IEMDC.1999.769087]

Ha, K.H., Kim, Y.K., Lee, G.H., Hong, J.P., 2004. Vibration reduction of switched reluctance motor by experimental transfer function and response surface methodology. *IEEE Trans. Magn.*, **40**(2):577-580. [doi:10.1109/TMAG.2004.825028]

Lecointe, J.P., Romary, R., Brudny, J.F., McClelland, M., 2004. Analysis and active reduction of vibration and acoustic noise in the switched reluctance motor. *IEE Proc.-Electr. Power Appl.*, **151**(6):725-733. [doi:10.1049/ip-epa:20040682]

Long, S.A, Zhu, Z.Q., Howe D., 2001. Vibration behaviour of stators of switched reluctance motors. *IEE Proc.-Electr. Power Appl.*, **148**(3):257-264. [doi:10.1049/ip-epa:20010255]

Long, S.A., Zhu, Z.Q., Howe, D., 2005. Effectiveness of active noise and vibration cancellation for switched reluctance machines operating under alternative control strategies. *IEEE Trans. Energy Conv.*, **20**(4):792-801. [doi:10.1109/TEC.2005.853763]

Miller, T.J., 1993. Switched Reluctance Motor and Their Control. Oxford, UK.

Pollock, C., Wu, C.Y., 1997. Acoustic noise cancellation techniques for switched reluctance drives. *IEEE Trans. Ind. Appl.*, **33**(2):477-484. [doi:10.1109/28.568013]

Srinivas, K.N., Arumugam, R., 2004. Static and dynamic vibration analyses of switched reluctance motors including bearing, housing, rotor dynamics, and applied loads. *IEEE Trans. Magn.*, **40**(4):1911-1919. [doi:10.1109/TMAG.2004.828034]

Sun, J.B., Zhan, Q.H., Wang, S.H., Ma, Z.Y., 2007. A novel radiating rib structure in switched reluctance motors for low acoustic noise. *IEEE Trans. Magn.*, **43**(9):3630-3637. [doi:10.1109/TMAG.2007.902604]

Tang, Y., 1997. Characterization numerical analysis, and design of switched reluctance motors. *IEEE Trans. Ind. Appl.*, **33**(6):1544-1552. [doi:10.1109/28.649967]

Wu, C.Y., Pollock, C., 1995. Analysis and reduction of vibration and acoustic noise in the switched reluctance drive. *IEEE Trans. Ind. Appl.*, **31**(1):91-98. [doi:10.1109/28.363045]